

# BIOCHEMISTRY

© Copyright 2005 by the American Chemical Society

Volume 44, Number 3

January 25, 2005

## Articles

### Structural Properties of the Promiscuous VP16 Activation Domain<sup>†</sup>

Hendrik R. A. Jonker, Rainer W. Wechselberger, Rolf Boelens, Gert E. Folkers,\* and Rob Kaptein

Bijvoet Center for Biomolecular Research, section NMR spectroscopy, Utrecht University,  
Padualaan 8, 3584 CH, Utrecht, The Netherlands

Received August 9, 2004; Revised Manuscript Received October 22, 2004

**ABSTRACT:** Herpes simplex virion protein 16 (VP16) contains two strong activation regions that can independently and cooperatively activate transcription *in vivo*. We have identified the regions and residues involved in the interaction with the human transcriptional coactivator positive cofactor 4 (PC4) and the general transcription factor TFIIB. NMR and biochemical experiments revealed that both VP16 activation regions are required for the interaction and undergo a conformational transition from random coil to  $\alpha$ -helix upon binding to its target PC4. The interaction is strongly electrostatically driven and the binding to PC4 is enhanced by the presence of its amino-terminal domain. We propose models for binding of VP16 to the core domains of PC4 and TFIIB that are based on two independent docking approaches using NMR chemical shift changes observed in titration experiments. The models are consistent with results from site-directed mutagenesis and provide an explanation for the contribution of both acidic and hydrophobic residues for transcriptional activation by VP16. Both intrinsically unstructured activation domains are attracted to their interaction partner by electrostatic interactions, and adopt an  $\alpha$ -helical conformation around the important hydrophobic residues. The models showed multiple distinct binding surfaces upon interaction with various partners, providing an explanation for the promiscuous properties, cooperativity, and the high activity of this activation domain.

Eukaryotic gene transcription by RNA polymerase II requires the assembly of many proteins on the promoter region (1–3). The rate of transcription is enhanced by transcriptional activators, through recruitment of chromatin remodeling enzymes and through facilitating the assembly of the preinitiation complex (PIC)<sup>1</sup> (4, 5). One of the best characterized activators is the herpes simplex virion protein 16 (VP16), also known as Vmw65, ICP25, or  $\alpha$ -TIF (6, 7). The carboxy-terminal region (residues 410–490) of this protein contains two potent transcription activation domains

(TADs) (8, 9) that can target many proteins of the RNA polymerase II transcription machinery, such as TBP (10), TFIIA (11, 12), TFIIB (13), the RAP74 subunit of TFIIF (14), the p62 component of TFIID (15), the TBP-associated-factors hTAF<sub>I</sub>31 (16), dTAF<sub>II</sub>40 (17), hTAF<sub>II</sub>32 (18), the human cofactor PC4 (19, 20), CBP (21, 22), and p300 (23, 24). The two functional regions in this acidic VP16 activation domain (VP16ad) are independently able to activate transcription *in vivo* via distinct pathways (8, 17, 22, 25–27). Both subdomains, VP16ad/n (412–453) and VP16ad/c (454–490), have been extensively studied by mutational analysis, indicating key roles for specific hydrophobic and acidic residues (26–29). The TADs of transcription factors often lack a folded structure under physiological conditions

<sup>†</sup> This work is supported by financial assistance from The Netherlands Organization for Scientific Research (NWO).

\* Corresponding author. Telephone: +31-(0)30-253-9930; fax: +31-(0)30-253-7623; e-mail: g.folkers@chem.uu.nl.

(30, 31). These and other native highly flexible random-coil proteins are identified as intrinsically unstructured proteins (IUPs). Previous structural studies of VP16ad showed that there is little evidence of secondary structure for the free protein (16, 32, 33). However, upon binding of a VP16 peptide (469–485) to the hTAF<sub>II</sub>31 (1–181), the 472–483 region becomes  $\alpha$ -helical (16). We have studied VP16ad by NMR and confirm that it is unstructured in solution. Both TADs are affected by interaction with PC4 and TFIIB. Upon binding to PC4, chemical shift perturbations and distinct NOE contacts, indicative for an  $\alpha$ -helical structure, are observed in both VP16 activation subdomains. We propose models for binding of VP16 to PC4 or TFIIB that are based on two independent docking approaches using NMR chemical shift data. The models are in agreement with results from mutational analysis and reveal different VP16 interaction surfaces. These results show the high adaptability of the flexible VP16ad to induce structure by interaction with the structurally distinct binding surfaces of PC4 and TFIIB.

## MATERIALS AND METHODS

**Preparation and Cloning of VP16ad, PC4, and TFIIB.** The VP16 and PC4 proteins were prepared and quantified essentially as described before (Jonker et al., submitted for publication, 34, 35). Uniformly labeled ( $^{15}\text{N}$ ,  $^{15}\text{N}/^{13}\text{C}$ ) VP16ad (residues 412–490) was obtained by using 0.5 g/L  $^{15}\text{NH}_4\text{Cl}$  (Isotec) and either 4.0 g/L  $^{12}\text{C}$ -glucose or 1.6 g/L  $^{13}\text{C}$ -glucose (Isotec) as the only nitrogen and carbon sources in minimal media (4.4 g/L  $\text{KH}_2\text{PO}_4$ , 10.4 g/L  $\text{K}_2\text{HPO}_4 \cdot 3\text{H}_2\text{O}$ , 50 mg/L  $\text{MgSO}_4 \cdot 7\text{H}_2\text{O}$ , 7 mg/L Mohr's salt, 10 mg/L thiamine, 50 mg/L ampicillin, and 40 mg/L chloramphenicol). Point mutants were made by PCR using a mutant primer containing a restriction site present in VP16 (StyI or SphI) and a primer of the plasmid backbone. The corresponding mutant fragments were subsequently cloned in pGEX 2T (ABP). The human TFIIB (111–316) fragment was generated by PCR and cloned in the NdeI and BamHI sites of pET15B (Novagen). All constructs were verified by sequencing. Overexpression and protein purification of the His-tag containing proteins was performed as described before (36).

**GST-Pull-Down Assays.** Purification of GST-fusion proteins was performed in batch at 4 °C according to the instructions of the supplier (ABP). The GST-beads were extensively washed with 50 mM Tris-HCl (pH 8.0) containing 50 mM NaCl, and subsequently 3 times with 20 mM potassium phosphate buffer (pH 6.2) containing 50 mM KCl. Binding experiments were performed in 400  $\mu\text{L}$  binding

buffer (20 mM potassium phosphate buffer (pH 6.2) containing 50 mM KCl, 0.2 mM PMSF, 1 mM DTT and supplemented with 0.2  $\mu\text{g}/\mu\text{L}$  BSA) with 2  $\mu\text{g}$  of GST-VP16 bound to GST-beads in the presence of the indicated amounts of PC4. Reaction mixtures were incubated for 2 h at 20 °C and washed 4 times with 500  $\mu\text{L}$  of binding buffer. Dry GST-beads were resuspended in SDS sample buffer and loaded on a 12.5% SDS–polyacrylamide gel. To be able to quantify the binding affinity, a known amount of PC4 was loaded onto the SDS–polyacrylamide gel next to the GST-pull-down experiments. For determination of the apparent  $K_d$  for the VP16–PC4 complex, binding was performed in a volume ranging from 100  $\mu\text{L}$  to 50 mL containing a constant amount of protein (ranging from 4 to 32  $\mu\text{g}$  in the different experiments). The more common approach of changing protein concentration, resulted in qualitatively identical results; however, due to detection problems, this approach did not allow us to accurately determine binding constants. After quantification of the retained PC4 protein using a Molecular Imager FX system using the software Quantity One (Bio-Rad), the apparent  $K_d$  was determined by fitting the binding data using nonlinear regression against bound fraction =  $1/(1 + (K_d/\text{[protein]})^n)$ . Analysis of the binding data from three experiments revealed a Hill-constant ( $n$ ) of 1 (within the experimental error), suggesting a 1:1 complex between the PC4 dimer and VP16.

**NMR Spectroscopy.** NMR experiments using 0.2 to 1 mM VP16ad were carried out at 298 K in 50 mM phosphate buffer (pH 5.6), containing 50 mM KCl (400 mM for PC4ctd to avoid aggregation), 2 M D<sub>5</sub>-glycine (for better long-term stability of the PC4 protein at higher temperatures (35)) or 5% D<sub>2</sub>O (for the VP16–TFIIB titration) and complete protease inhibitor (Roche). NMR experiments were performed essentially as described in Cavanagh et al. (37) on Varian Inova 500, 750 and Bruker Avance 500, 600 and 750 MHz spectrometers using triple-resonance probes. Titration experiments were performed by adding increasing amounts (1–80  $\mu\text{L}$ ) of concentrated (>1 mM) unlabeled protein to 450  $\mu\text{L}$  of  $^{15}\text{N}$ -labeled VP16ad sample (0.2 mM), both in the same buffer solution. While the biochemical experiments were performed with wild-type VP16ad, the NMR experiments have been performed with a mutant M470T as well as wild-type VP16ad. For unknown reasons, the stability of a M470T point mutant in complex with PC4 was better than the wild-type protein for NMR conditions and therefore used for the resonance assignment. Titration experiments using both versions revealed essential identical chemical shift changes upon interaction with PC4. The resonances for wild-type VP16ad were assigned by overlaying the ( $^1\text{H}, ^{15}\text{N}$ )-HSQC spectra and by verification of NOE patterns from 3D NOESY-( $^1\text{H}, ^{15}\text{N}$ )-HSQC spectra. NMR experiments performed for the resonance assignment of VP16ad were 3D HNCA, 3D HN(CO)CA, 3D CBCANH, CBCA(CO)NH, 3D HNCO and 3D HN(CA)CO, 3D NOESY-( $^1\text{H}, ^{15}\text{N}$ )-HSQC and 3D TOCSY-( $^1\text{H}, ^{15}\text{N}$ )-HSQC. The spectra were processed using the software package NMRPipe (38) and analyzed using SPARKY 3 (T. D. Goddard and D. G. Kneller, University of California, San Francisco).

**Molecular Modeling Using BiGGER and HADDOCK.** Initial molecular modeling was performed with BiGGER (39, 40) using 15° angular steps for the full  $\alpha$ -helical VP16ad on PC4ctd and TFIIBc, and a rotation of 10° in all the other

<sup>1</sup> Abbreviations: BiGGER, biomolecular complex generation with global evaluation and ranking; CBP, CREB binding protein; CREB, cyclic-AMP response element binding protein; CSI, chemical shift index; GST, glutathione S-transferase; HADDOCK, high ambiguity driven protein–protein docking; HSQC, heteronuclear single-quantum coherence; NOE, nuclear Overhauser enhancement; NOESY, NOE spectroscopy; PC4, human positive cofactor 4; PC4ntd, PC4ctd: amino or carboxy terminal domain of PC4; PDB, Protein Data Bank; PIC, preinitiation complex; PSSI, probability based secondary structure identification; RAP74, RNA polymerase-associated protein 74 (TFIIF $\alpha$ ); TAD, transcription activation domain; TALOS, torsion angle likelihood obtained from shift and sequence similarity; TAFII, TBP associated factor; TBP, TATA-box binding protein; TFIIB, transcription factor II; TOCSY, total correlation spectroscopy; VP16, herpes simplex virion protein 16, ( $\alpha$ -TIF, ICP25, and VMW65); VP16ad, VP16 activation domain; VP16ad/n, VP16ad/c: amino or carboxy terminal part of VP16ad.

cases. The dockings were performed using the crystal structure of the PC4ctd dimer (41), the closest to average NMR structure of TFIIBc (42) and VP16ad  $\alpha$ -helices, created with Swiss Pdb Viewer 3.7 (43). The best 5000 binding modes are kept on the basis of the geometric complementarity and amino acid pairwise affinity across the complex interface. These solutions are evaluated in terms of a global scoring function on the basis of surface matching, electrostatic interactions, side-chain contacts across the molecular interface, and the relative desolvation energy. The residues that showed a significant chemical shift perturbation (or line broadening) in NMR titration experiments are used to filter the docking results. The docking models are ranked on basis of the number of atomic contacts within a 5 Å distance cutoff between the selected residues of both partner proteins. Similar solutions are clustered within a threshold of 2.0 Å (PC4ctd) and 2.6 Å (TFIIBc) and treated as one unique binding mode. The closest to average of the top-ranked cluster was accepted as the best representative orientation. The best docking results were subsequently energy minimized using the GROMOS96 43B1 force field (44) implemented in Swiss-Pdb Viewer 3.7 (43).

The docking results have been verified and optimized using a high ambiguity driven protein–protein docking (HADDOCK) approach essentially as described by Dominguez et al. (45). The ambiguous interaction restraints (AIRs) have been defined for the residues that exhibited significant chemical shift changes upon interaction with TFIIBc (46) or PC4 (Jonker et al., manuscript in preparation). Residues in one of the two symmetrical binding sites of the PC4ctd dimer and the preferential binding groove of TFIIBc have been selected for the dockings to avoid too much ambiguity. Dockings have been performed with the full-length, 430–450 or 465–490 region of VP16ad to TFIIBc or the PC4ctd dimer. The final docking results for PC4ctd and TFIIBc are clustered at the interface within a threshold of 2.0 or 2.6 Å pairwise backbone RMSD, respectively. The top ranked ensemble, according to the average interaction energy and buried surface area, was accepted as the best representative of the complex. Intermolecular hydrogen bonds and contacts were determined using HADDOCK and MOLMOL (47) analysis. Hydrogen bonds are considered when frequent contacts between donor and acceptor are observed for the cluster within a distance of 2.5 Å. Hydrophobic and electrostatic contacts are defined when the distance between the van der Waals surfaces is less than 1.0 Å.

## RESULTS

**Resonance Assignment of the VP16 Activation Domain.** Previous studies indicated that VP16ad is unstructured in solution and evidence has been presented that suggests the formation of an ordered structure upon interaction to specific target proteins (16, 32, 33). To study the nature and structural properties of VP16ad in detail by NMR, triple resonance spectra of doubly labeled ( $^{13}\text{C}/^{15}\text{N}$ ) VP16ad have been recorded for sequential assignment of the  $^1\text{H}$ ,  $^{15}\text{N}$ , and  $^{13}\text{C}$  resonances. Despite the small dispersion in the proton dimension (<1 ppm) and multiple overlapping peaks, all the backbone amide signals in the ( $^1\text{H}, ^{15}\text{N}$ )-HSQC could be assigned for residues 412 to 490. The chemical shift values

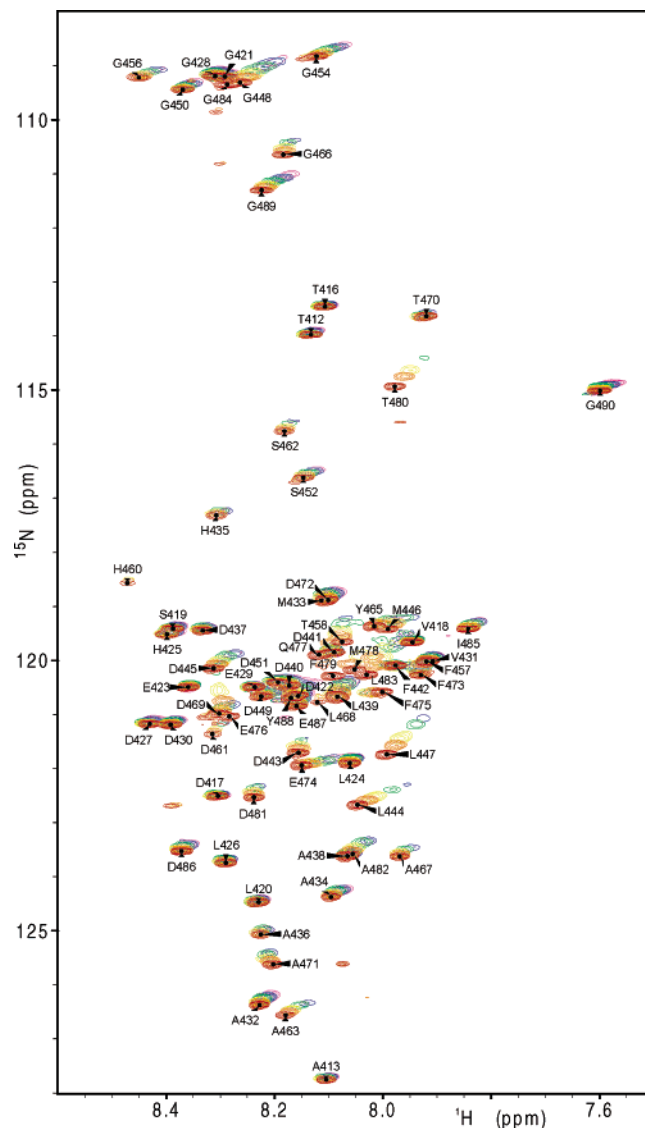


FIGURE 1: Overlay of the ( $^1\text{H}, ^{15}\text{N}$ )-HSQC spectra (500 MHz) of the VP16ad (M470T mutant) titration with full-length PC4. Spectra are presented for the free form (red) and for molar ratios (PC4: VP16) of 1:0.4 (orange), 1:0.8 (yellow), 1:1.2 (green), 1:1.8 (blue) and 1:2.5 (purple). The backbone assignments are indicated for VP16ad in the free form. The spectra were acquired at 298 K in a phosphate buffer (50 mM KCl, 50 mM  $\text{KH}_2\text{PO}_4$ ; pH 5.6, 2 M  $d_5$ -glycine).

of VP16ad have been deposited in the BioMagResBank under accession number 6099.

**Identification of the VP16ad Interaction Regions.** To study the regions of the VP16 activation subdomains involved in the interaction with distinct target proteins, NMR titration experiments have been performed using  $^{15}\text{N}$ -labeled VP16ad with unlabeled proteins, known to be involved in the RNA polymerase II transcription. We have studied the interaction of VP16ad with the general transcriptional cofactor PC4, the carboxy-terminal core domain of PC4 (PC4ctd, residues 62–126), and the amino-terminal regulatory domain of PC4 (PC4ntd, residues 1–63). An overlay of ( $^1\text{H}, ^{15}\text{N}$ )-HSQC spectra of the titration with full-length PC4 is shown in Figure 1. Furthermore, titration experiments were carried out with the unlabeled carboxy-terminal core domain of TFIIB (TFIIBc; 112–316). The titration experiments show progressive changes of the amide  $^1\text{H}$  and  $^{15}\text{N}$  chemical shifts, indicative for fast exchange between the bound and free states

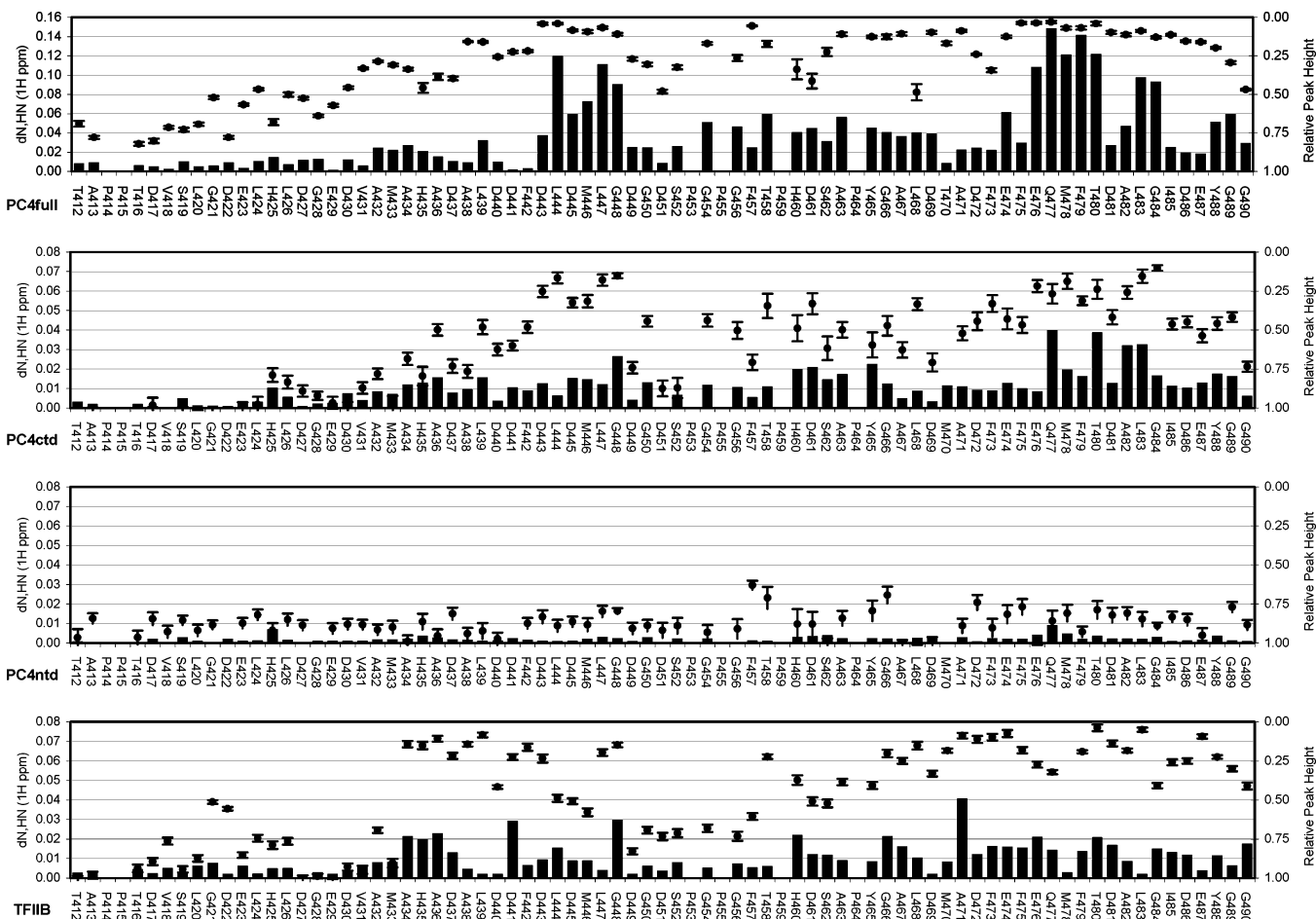


FIGURE 2: Chemical shift perturbations and decrease of signal intensity in VP16ad ( $\sim 200 \mu\text{M}$ ) due to an excess addition of full-length PC4 (as in Figure 1), and an equimolar amount of PC4ctd, PC4ntd, and TFIIBc, until no more changes were observed and the signals of the most affected residues could still be unambiguously assigned. The amide  $^1\text{H}$  and  $^{15}\text{N}$  resonance shifts have been mapped and combined as Euclidian distances between peak maxima (in  $^1\text{H}$  ppm), presented as bars with respect to the primary y-axis on the left. The peak heights of the amide signals after addition of the unlabeled partner protein have been divided by the peak heights before addition. These relative peak heights are presented as dots with error bars (calculated from the rms baseline noise) with respect to the secondary inverted y-axis on the right side of the graphs.

on the NMR time scale. Despite the overlap and line-broadening effects, the chemical shift changes could be mapped unambiguously. The unfavorable NMR behavior unable us to determine the stoichiometry of the complex. The backbone amide perturbations for the titrations with TFIIIBc, full-length PC4, PC4ctd, and PC4ntd are presented in Figure 2.

The titration experiment of the  $^{15}\text{N}$ -labeled VP16ad with unlabeled PC4ntd revealed no significant changes in the ( $^1\text{H}, ^{15}\text{N}$ )-HSQC, suggesting that the two proteins did not or very weakly interact. Nevertheless, the presence of PC4ntd enhances the VP16–PC4 interaction as is clearly indicated by the larger chemical shift perturbations observed in the NMR titration experiment for VP16ad with full-length PC4 in comparison with PC4ctd at equimolar ratios. PC4ntd specifically stimulates the VP16–PC4 interaction for most residues in the 444–448 and 474–484 regions in VP16ad as we observe 2–3-fold increased chemical shift changes in these regions for the VP16ad–PC4 versus the VP16ad–PC4ctd interaction.

Two distinct regions in VP16ad are affected by the interactions with both TFIIB and PC4. The most significant chemical shift change and line broadening is observed in the 430–450 and 460–490 regions. To confirm the contri-

bution of both regions for the interaction with PC4, GST-pull-down assays were performed using VP16 deletion constructs and full-length PC4. As shown in Figure 3A, wild-type PC4 can interact with full-length VP16 ( $K_d = 0.7 \pm 0.2 \mu\text{M}$ ), and both regions are mostly indispensable for the interaction. The VP16ad/n subdomain failed to interact with PC4, while the VP16ad/c region binds at least 20 times weaker ( $K_d = 15 \pm 6 \mu\text{M}$ ).

*Mutational Analysis of VP16ad Binding to PC4.* The VP16ad regions involved in the interaction contain a large number of acidic residues that provide a strong negatively charged binding surface. Mutagenesis studies of positively charged residues in the PC4 interaction area and phosphorylation of the PC4 indicated that the binding is strongly electrostatically driven (Jonker et al, manuscript in preparation). To verify that the VP16 residues, identified by NMR, are involved in the interaction with PC4, specific point mutants have been designed in both VP16ad binding regions (Figure 3B). Two negatively charged aspartate (D443, D445) residues in the first region (VP16ad/n) have been mutated to alanine (neutral charge) or lysine (positive charge). Compared to the wild-type VP16-PC4, a 20% and 45% decrease in binding was observed for the alanine and the lysine mutation, respectively. A similar result was observed

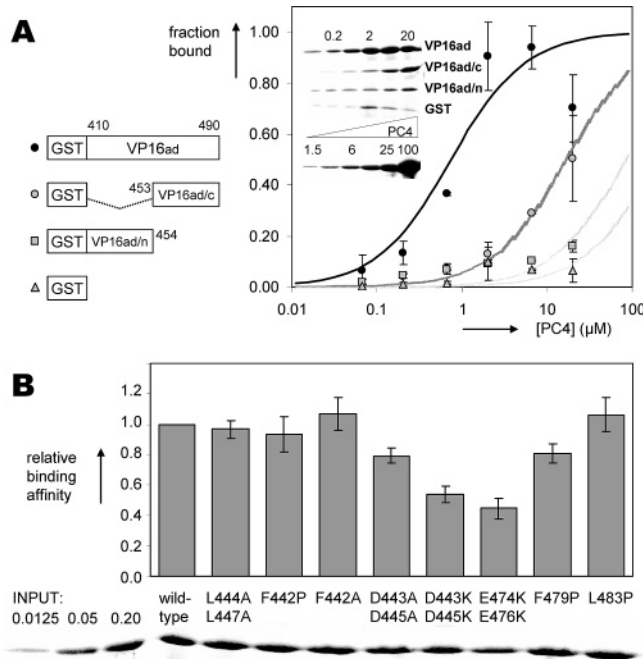


FIGURE 3: The acidic regions of the two activation domains of VP16 are required for high-affinity binding to PC4. (A) Average of three independent GST-pull-down experiments using the indicated PC4 concentration with the indicated GST-VP16 deletion constructs. The interactions are calculated relative to the PC4 concentration where the strongest interaction with GST-VP16 was detected (set at 1). The inset shows Coomassie-stained SDS-polyacrylamide gels from representative GST-pull-down assays in the presence of 0.07, 0.2, 0.7, 2, 6.7, and 20 μM PC4. In the lower panel, a SDS-polyacrylamide gel is shown with 1.5, 3, 6, 12.5, 25, and 100% of the total PC4 added to the binding experiments. (B) In vitro binding studies of specific VP16ad point mutants to full-length PC4. Quantification of four GST-pull-down experiments using the indicated VP16ad mutants relative to the interaction between wild-type GST-VP16 and PC4 (set at 1). The lower panel shows a representative GST-pull-down experiment in the presence of 1 μM PC4. For comparison 1.25, 5, and 20% of PC4 added to the interaction was loaded next to these experiments (input).

in the second region (VP16ad/c) where two negatively charged glutamates (E474 and E476) were mutated to positively charged lysine residues, resulting in more than 50% reduction of PC4–VP16 complex formation.

The conserved hydrophobic residues F442 and L444 in the VP16ad/n subdomain have been shown to be critical for transcription activation (26, 28). The amide signals of L444 and L447 show significant chemical shift perturbations upon binding to PC4 (Figure 2). To investigate whether these residues affect PC4 binding, we examined the binding affinity of a single point mutant F442A and a double point mutant L444A,L447A. No significant decrease in binding affinity is observed for the F442A mutant and only a minor decrease for the double L444A,L447A mutant.

Since α-helical properties might be important for the interaction (16), we designed specific point mutations in the center of both transcription activation subdomains that would disrupt the putative α-helix. F479, L483, and F442 have been replaced by a proline residue. No decrease in PC4 binding affinity was observed for L483P. This residue is located on the edge of the main interaction region (residues 474–484). Only a small decrease in binding affinity is observed for F442P, that is also located just outside the 443–448 area that was found to be of major importance for interaction with

PC4. For the F479P point mutation, a significant decrease of 20% in binding affinity is observed.

**Structural Properties of the VP16 Activation Domain.** The (<sup>1</sup>H,<sup>15</sup>N)-HSQC spectrum of VP16ad shows a small dispersion of intense signals in the proton dimension (<1 ppm), indicative for a lack of secondary structure. This has previously been observed in a <sup>1</sup>H NMR study (32). Probability based secondary structure identification using all the available <sup>1</sup>H, <sup>15</sup>N, and <sup>13</sup>C chemical shifts, with PSSI (48), CSI (49), and TALOS (50) show that these resonances are around the random coil positions, confirming that VP16ad exhibits hardly any secondary structure. The <sup>13</sup>C<sub>α</sub>, <sup>13</sup>C', and <sup>1</sup>H<sub>α</sub> resonances, which are most indicative to distinguish an α-helix from a random coil (48), indicate only a marginal α-helical content in the 431–449 and 467–487 regions, suggesting that the α-helical conformation might be occasionally populated.

NMR titration experiments show that the amide <sup>1</sup>H and <sup>15</sup>N resonances shift toward lower ppm values, indicating formation of α-helical structure elements (49). To verify secondary structure formation for VP16ad in complex, another titration experiment was performed using doubly labeled (<sup>13</sup>C/<sup>15</sup>N) VP16 with full-length unlabeled PC4. For the titrations of <sup>15</sup>N-labeled VP16 with PC4 (Figures 1 and 2), we observed broadening and disappearance of peaks due to the formation of a larger complex and exchange between the PC4-bound and free VP16ad. Although the exact stoichiometry of the VP16–PC4 complex is unknown, based on the known PC4 dimer (14.3 kDa each) and a single VP16ad (8.4 kDa) molecule, a complex of at least a 37 kDa is formed, a molecular weight increase of more than a factor of 4. Furthermore, NMR relaxation data as well as analytical gel filtration experiments (data not shown) suggest that an even higher order complex of two to four PC4 dimers with one or two VP16 molecules can be formed. Since carbon labeling causes additional peak broadening, signals will largely disappear before we reach the full complex. Therefore, at molar ratios of 1:320, 1:160, 1:80, 1:40, 1:20, and 1:10 (monomer PC4:VP16), (<sup>1</sup>H,<sup>15</sup>N)-HSQC, 2D-HNCACB, and 2D-HNCO spectra have been recorded to map the <sup>13</sup>C chemical shift changes. The <sup>13</sup>C resonances could be mapped unambiguously until the addition of 10% unlabeled PC4 (1:10). After addition of 15% PC4 (1:6.6), some signals of the most affected residues have disappeared or could not be unambiguously assigned due to overlap. 3D NOESY-(<sup>1</sup>H,<sup>15</sup>N)-HSQC spectra have been recorded before and after addition of 10% and 15% of the unlabeled PC4 to observe the H<sub>α</sub> chemical shift changes and sequential NOE contacts in the bound form.

The <sup>1</sup>H<sub>N</sub>, <sup>15</sup>N, <sup>1</sup>H<sub>α</sub>, <sup>13</sup>C<sub>α</sub>, <sup>13</sup>C<sub>β</sub>, and <sup>13</sup>C' resonance shifts have been mapped for the complete VP16ad sequence and are presented in Figure 4. In both activation subdomains negative <sup>1</sup>H<sub>N</sub>, <sup>15</sup>N, and <sup>1</sup>H<sub>α</sub> as well as positive <sup>13</sup>C<sub>α</sub> and <sup>13</sup>C' resonance shifts are observed, indicative for α-helix formation. To analyze the overall effect of all the observed chemical shift changes upon complex formation, the resonance shifts were sign and nucleus specifically combined (Δall, see figure legend Figure 4). The positive values for Δall are indicative for the formation of an α-helix, while negative values would suggest the formation of a β-sheet. From these analysis, we can clearly observe the formation of α-helices in the 443–447 and 469–483 region (Figure

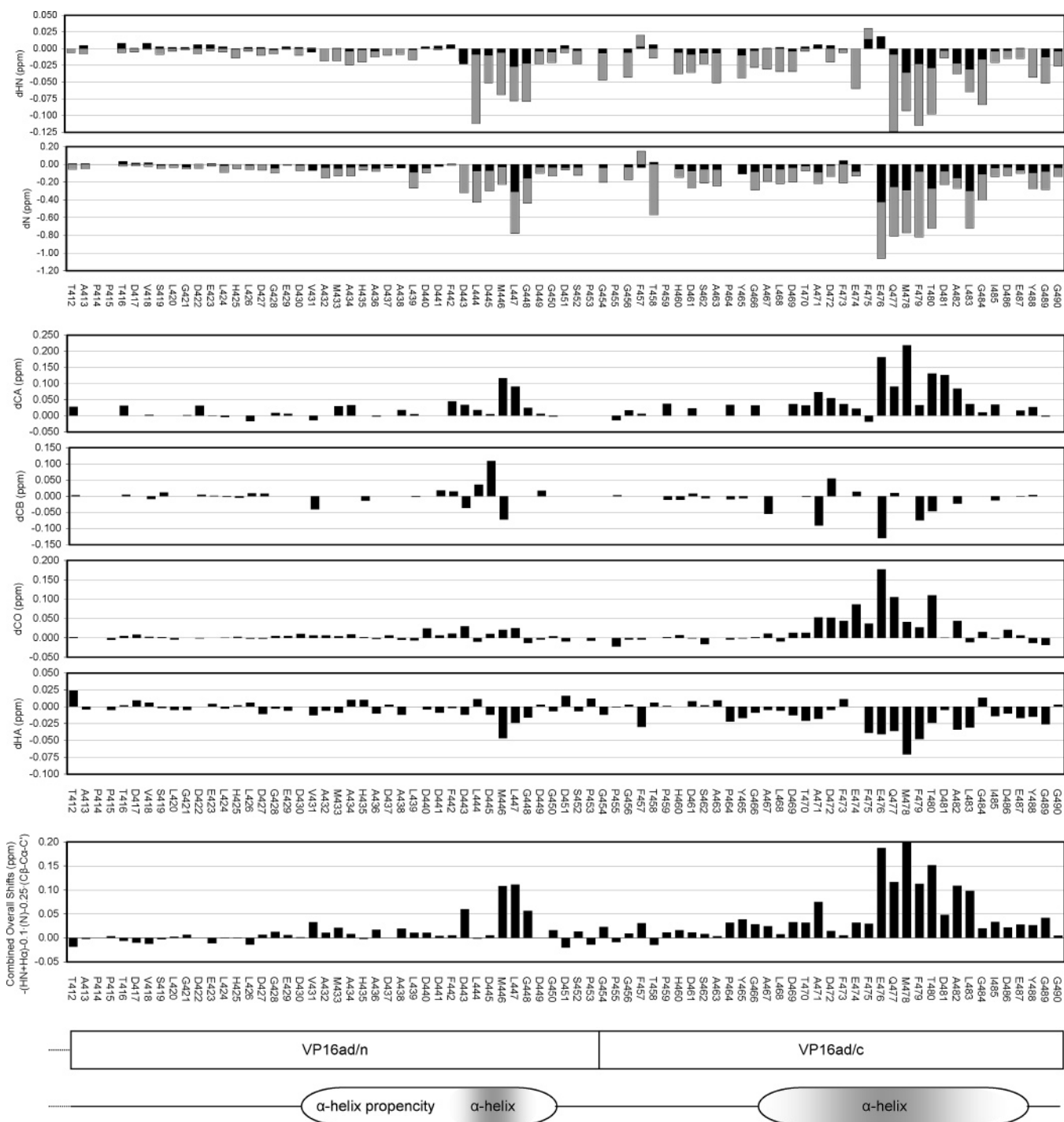


FIGURE 4: Chemical shift changes in the VP16 activation domain due to addition of full-length PC4. The perturbations in amide  $^1\text{H}$  and  $^{15}\text{N}$  resonances are shown for the titration of the doubly labeled ( $^{13}\text{C}/^{15}\text{N}$ ) VP16 sample after addition of about 15% PC4 (black bars) as well as for the titration of the  $^{15}\text{N}$  labeled VP16 sample with an excess of PC4 (gray bars). The  $^1\text{H}\alpha$  shifts are shown after addition of about 15% PC4 and the  $^{13}\text{C}_\alpha$ ,  $^{13}\text{C}_\beta$ , and  $^{13}\text{C}'$  shifts after addition of 10% PC4. The chemical shift perturbations for the doubly labeled titration experiment have been sign-specifically combined, taking the gyromagnetic ratio of the nuclei into account ( $\Delta_{\text{all}} = -(\Delta\delta_{\text{HN}} + \Delta\delta_{\text{HO}}) - 0.1(\Delta\delta_{\text{N}}) - 0.25(\Delta\delta_{\text{C}\beta} - \Delta\delta_{\text{C}\alpha} - \Delta\delta_{\text{C}'})$ ), to indicate the (positive) changes toward  $\alpha$ -helix formation. This formula is based on the resonance combination used by Vis et al (71) with modifications.

4), especially since we have to take into account that resonances have only been mapped until a 1:10 complex. The perturbations for a 1:1 complex would have been much larger, as shown by the corresponding amide  $^1\text{H}$  and  $^{15}\text{N}$  resonance shifts for the titration experiment using  $^{15}\text{N}$ -labeled VP16ad, which could be followed until an excess of full-length PC4 was present. The  $^{13}\text{C}_\beta$  resonance shifts of in particular D445, M446, A467, A471, D472, E476, and F479 may indicate the involvement of the side-chain for the

interaction with PC4. In the 3D NOESY-( $^1\text{H}, ^{15}\text{N}$ )-HSQC, we can observe a large perturbation ( $-0.2$  ppm) of the  $^1\text{H}_\beta$  values of F479, suggesting that this phenylalanine side-chain is specifically involved in the interaction, which is in agreement with the observed decrease in binding affinity for the F479P point mutation (Figure 3B).

To verify the formation of  $\alpha$ -helical structural elements in VP16ad, we compared the 3D NOESY-( $^1\text{H}, ^{15}\text{N}$ )-HSQC spectra before and after addition of full-length PC4. Although

the final complex is not reached, a substantial number of weak NOE contacts can be observed (Figure 5A). In the bound form, specific contacts (such as  $d_{\text{NN}}(i,i+2)$ ,  $d_{\alpha\text{N}}(i,i+3)$ , and  $d_{\beta\text{N}}(i,i+3)$ ) can be observed, which are indicative for an  $\alpha$ -helical structure. Some weak, but potential  $d_{\alpha\text{N}}(i,i+4)$  contacts can also be observed, although they are hard to unambiguously assign because of overlap. The NOE contacts of the complex are summarized in Figure 5B. However, we cannot confirm the presence of all the expected contacts due to largely overlapping peaks. Missing contacts in the 475–480 region are mostly caused by the decrease in signal intensity due to extensive peak broadening as a result of the large complex formation or exchange. Nevertheless, the NOE patterns clearly indicate that VP16ad exhibits an  $\alpha$ -helical propensity throughout the sequence, except for the proline-rich 453–464 region. Many NOE contacts, indicative for an  $\alpha$ -helix, are observed for residues 429–450 and 465–488 in both subdomains.

**Docking of TFIIBc and PC4ctd to an  $\alpha$ -Helical VP16ad.** NMR titration experiments of VP16ad with full-length PC4 indicate formation of  $\alpha$ -helical regions in VP16ad. Comparable chemical shift changes were observed for the interaction with TFIIBc, suggesting similar  $\alpha$ -helix formation in VP16ad. Biochemical and NMR titration experiments of VP16 with PC4 and TFIIB reveal the involvement of particular charged residues in the VP16ad interaction site. The PC4ctd interaction site for VP16ad has been evaluated before (Jonker et al, manuscript in preparation) and involves mostly the positively charged lysine and arginine residues in the  $\beta$ -channel region. Furthermore, the VP16ad interaction surface of TFIIBc has been determined by protease footprinting (51), NMR (46), small-angle X-ray scattering (33), and site-directed mutagenesis (52–54). Together with the interaction surfaces of the two VP16ad subdomains for interaction with PC4 and TFIIB, as determined by NMR titration experiments (Figures 2 and 4) and site-directed mutagenesis (Figure 3), models for the PC4ctd–VP16 and TFIIB–VP16 complexes can be made. Therefore, dockings have been performed with BiGGER (39, 40) and HADDOCK (45) with a variety of VP16ad  $\alpha$ -helical regions (different in length and position) to the TFIIBc and PC4ctd core domains. Using BiGGER, the core domains of TFIIB and PC4 have been docked on a completely  $\alpha$ -helical VP16ad to verify the preferential binding site for both proteins. Figure 6A shows the best 500 results from this docking on the basis of the global scoring. Both TFIIBc and PC4ctd are predicted to bind preferentially to the 465–485 region of VP16, and clearly less preferable interaction is suggested for the VP16ad/n region. This is in agreement with the observed binding affinities of both subregions for PC4 (Figure 3A) and fluorescence analyses in TFIIB (55).

**Model of the VP16ad-PC4ctd Complex.** The BiGGER and HADDOCK docking results for the VP16 465–490 region onto the PC4ctd dimer (Figure 6B) show a preferential binding toward the positively charged residues in the  $\beta$ -channels and  $\beta_2$ – $\beta_3$  loop region. Both docking approaches reveal the same predominant orientation in which the 474–484 region, which has been shown to be mostly affected by binding, is particularly well enclosed underneath one of the  $\beta_2$ – $\beta_3$  arms of the PC4ctd dimer. The spread in docking ensembles observed in both protocols suggest that the complex maintains some intrinsic flexibility and freedom of

movement of the  $\alpha$ -helix. This is underscored by the interchangeable electrostatic contacts of adjacent negatively charged residues with the same positively charged residues of PC4. The positively charged side-chains of the R74, K77, K79, R85, K96, and R99 residues from the  $\beta$ -sheet and loop regions of PC4 reorientate during the HADDOCK water refinement and show close contacts to the negatively charged VP16ad surface made of D472, E474, E476, D481, D486, and E487 residues (most docking results show hydrogen bonds between PC4 and VP16 for residues K77/K79 and D481, R85 and E476/T480, K96 and D472/E476, R99 and D472/E474/E476). Residues S103, N105, Q108 in the  $\beta_4$ -sheet and start of the  $\alpha$ -helix and R69' and K100' from the opposite PC4 monomer further improve the electrostatic interaction, as hydrogen bonds are observed toward D486 or E487. In addition, hydrophobic contacts are observed for F76 and L81 (PC4) and F479, T480 and L483 (VP16). Highly similar docking results were obtained for the 430–450 region of VP16ad/n (data not shown), in which the  $\alpha$ -helical 440–448 region contacts the same PC4 residues as the 474–484 region of VP16ad/c.

**Model of the VP16ad-TFIIBc Complex.** Dockings of the VP16 465–490 region to TFIIBc indicate a strong preference for the groove formed by the C1, D1, and E1 helices in the first repeat of TFIIBc (Figure 6C). The negatively charged surface of the VP16  $\alpha$ -helix is spread over this positively charged groove. Both docking results show an ensemble with various contact possibilities. Many electrostatic contacts are observed between the VP16ad  $\alpha$ -helix and K200, K196, R193, K189, and K188 in the E1 helix and R286, Q287, R290, and R295 in the E2 helix of TFIIBc (hydrogen bonds between TFIIB and VP16 are often observed for K200 and D469, K196 and D469/D472, R193 and E474, K188 and D481, R290 and D472/E476). Hydrophobic contacts are observed for F473, F475, M478, F479, T480, and L483 (VP16) and residues in the C1 (Y165, A162), D1 (C181, F177), E1 (F195, I191), and E2 (V283, L291, Y293) helices of TFIIBc, which may stabilize the complex. Furthermore, contacts are observed toward K312 and the B2–C2 loop region (Y465–R248, L468–G247) of TFIIBc. Since both VP16 activation subdomains contribute to TFIIB binding (17), additional dockings were performed for VP16ad/n on either TFIIBc or the TFIIBc-VP16ad/c complex. These dockings show many possible orientations and binding sites. The VP16ad/n region is able to bind to the same region as VP16ad/c, but might as well contact the backside of the C1 helix or the A2–B2 helix of the second repeat, which might explain the chemical shift perturbations in these regions (46).

## DISCUSSION AND CONCLUSION

The VP16 activation domain is one of the most potent transcription activation regions described and is widely used as a model for the action of regulatory proteins and their interactions with the basal transcription machinery. NMR titration experiments (Figures 1 and 2) indicate that both VP16 activation subdomains are involved in the interaction with PC4 and TFIIBc. Deletion analysis shows that the VP16ad/n region fails to interact while VP16ad/c has a reduced binding affinity (>20 times compared to the full VP16ad) for PC4 (Figure 3A), indicating that both VP16

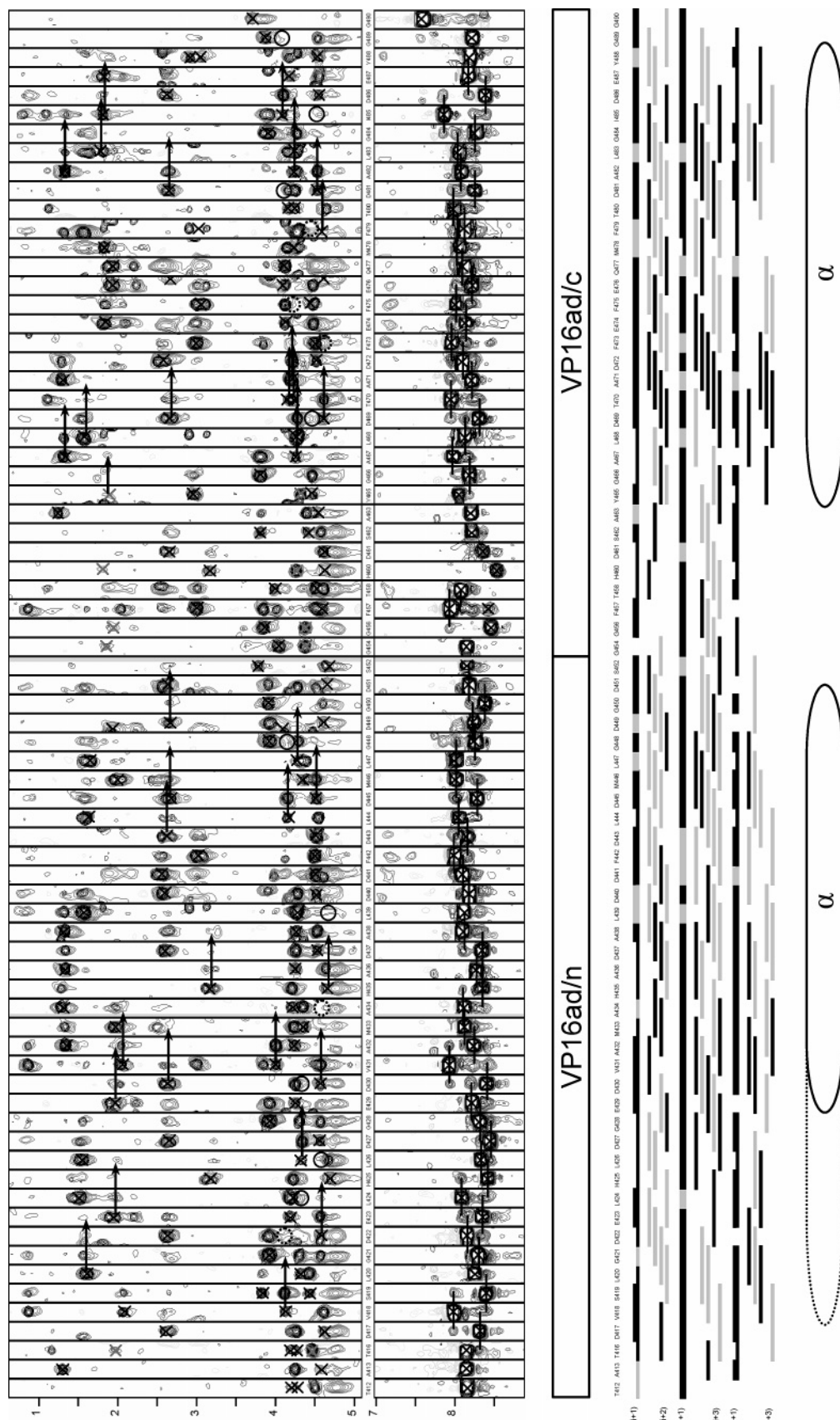


FIGURE 5: Overlay of the VP16ad strip plots from 3D NOESY- $(^1\text{H}, ^1\text{N})$ -HSQC spectra (750 MHz) before (black) and after (grey) addition of 15% PC4. Unambiguous  $d_{\alpha\text{N}}(i,i+3)$  and  $d_{\beta\text{N}}(i,i+3)$  contacts are marked by arrows. The  $d_{\text{NN}}(i,i+1)$   $d_{\text{NN}}(i,i+2)$  contacts have been marked by a line and potential  $d_{\alpha\text{N}}(i,i+4)$  contacts by a circle. The VP16 subdomains are indicated below, as well as a summary of the observed NOEs and the structure elements. Black lines indicate that an NOE cross-peak has been found and gray lines indicate overlap.

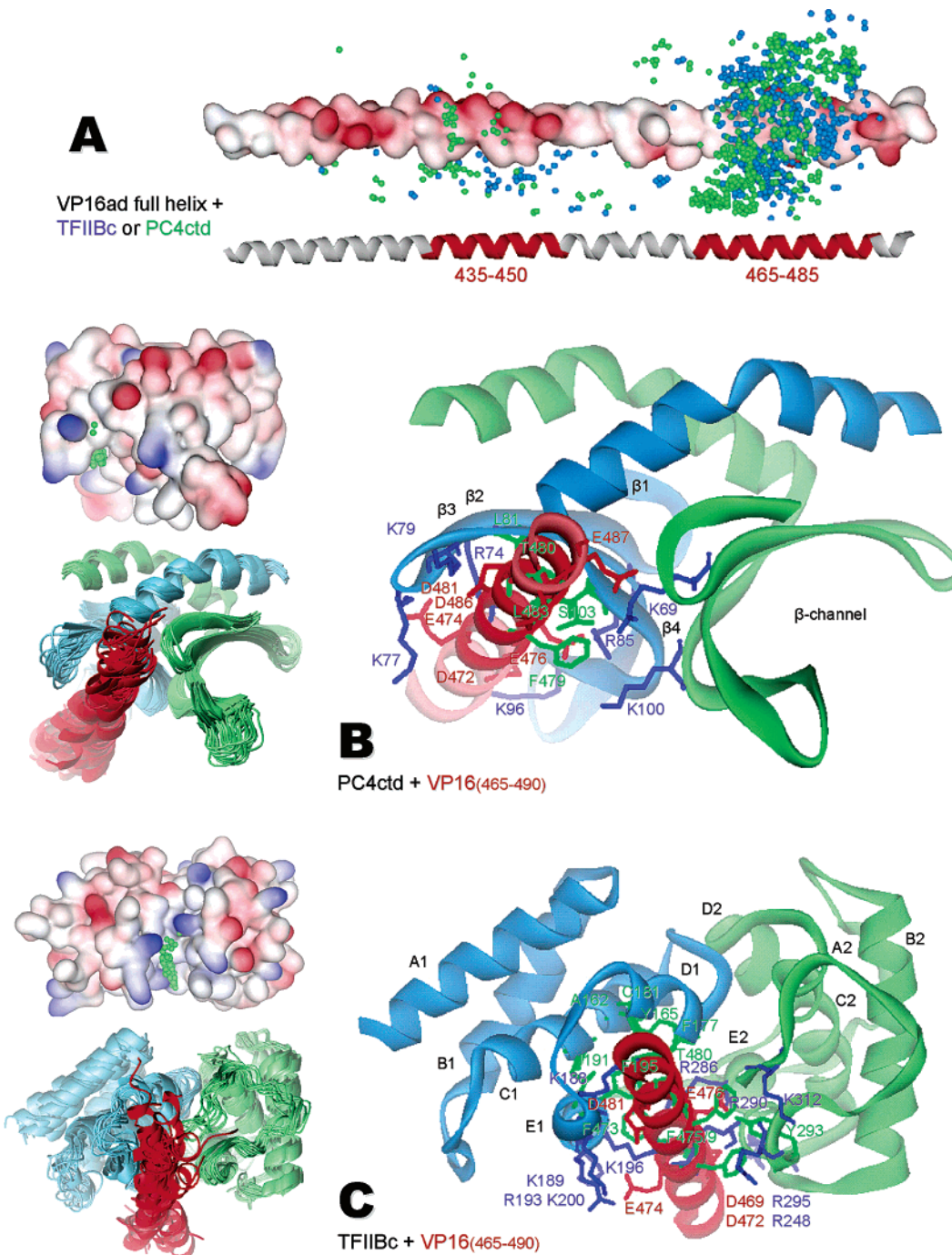


FIGURE 6: Docking results of TFIIBc and PC4ctd with VP16ad. (A) The 500 best BiGGER docking results (global scoring, dots represent the center of mass of the probe molecule) of TFIIBc (blue) and PC4ctd (green) on a full-length VP16ad  $\alpha$ -helix. Negative charges are presented in red on the VP16ad surface. The 435–450 and 465–485 regions, mostly involved in the interactions with TFIIBc and PC4ctd, are indicated on the ribbon diagram. BiGGER and HADDOCK dockings of the VP16 465–490 helix on the PC4ctd dimer (B) or TFIIBc (C). The best 100 (NMR filtered) BiGGER docking results are shown as green dots onto the PC4 or TFIIB surfaces (blue for positive and red for negative charges). The ribbon diagram shows the best representative of the predominant docking orientation (same orientation as the surface). The VP16 helix is shown in red and the two PC4ctd monomers or TFIIBc repeats in green and blue. Some specifically involved side-chains are indicated as dark blue (basic), red (acidic), or green (hydrophobic) sticks. The 20 energetically best structures from the top ranked 2.0 Å HADDOCK cluster are shown for PC4. For TFIIB, the 10 energetically best structures from the top-ranked 2.6 Å HADDOCK cluster are shown. Residues used to filter the BiGGER results are 66, 72, 74, 77–80, 83–85, 90, 100, 101, 103, 104, and 111 for PC4ctd, and 435, 436, 438, 439, 442–448, 450, and 454–489 for VP16ad. Residues 72, 74, 77–80, 83–85, 101, 103, 104, 66', and 100' (PC4ctd) and 444–448, 474, 476–480, 482–484, 488, and 489 (VP16ad) have been selected as active and 61, 62, 75, 76, 81, 87, 97–99, 102, 105, 106, 108, 67', 69', 86', 99', and 126' (PC4ctd) and the other residues in the 440–450 and 470–490 regions of VP16 as passive restraints for HADDOCK. Residues mapped by Hayashi et al (46) have been used as restraints for TFIIBc. Residues in the preferential binding groove have been selected as active and the closest surface neighbors as passive restraints for HADDOCK. The VP16ad residues 434–439, 441–444, 447, 448, 458, 460, 466–477, and 479–490 are used to filter the BiGGER results. Residues 434–436, 441, 444, 448, 466, 467, 471, 473–476, 480, 481, 484, and 490 are selected as active and the other residues in the 431–450 and 465–490 regions as passive restraints for the VP16 docking to TFIIB with HADDOCK. The pictures have been generated with MOLMOL 2k.2 (47) and ViewerLite 5.0 (Accelrys Inc.).

activation subdomains are required for high-affinity cooperative binding. Similar cooperativity is also observed for transcription (7, 8, 56). Significant resonance perturbations and a decrease in binding affinity upon mutation (Figure 3B) of negatively charged residues suggests a strong electrostatically driven binding mode. Sign-specific chemical shift changes (Figure 4) and distinct NOE contacts (Figure 5) indicate formation of  $\alpha$ -helices in both VP16ad regions upon binding to PC4. Docking experiments were performed for both activation subdomains with PC4 and TFIIB, showing that the residues important for transcription activation make interactions with the target protein.

**Helix Formation in the VP16 Activation Domain upon Interaction with PC4.** VP16 was shown before to be unstructured in solution (16, 32, 33). We confirm this notion by the absence of NOE contacts that are indicative for secondary structure elements. The chemical shift values, which are mostly around the random coil positions, indicate a slight propensity toward  $\alpha$ -helical structure in both VP16 activation subdomains. Similar limited sampling of the helical conformation in TADs was also seen for CREB (57) and p53 (58). Lack of structure is a well-known characteristic of TADs (30, 31). In a few cases, atomic details were obtained about TADs with their targets, and all revealed an induced  $\alpha$ -helix formation (16, 57, 59–62). Characteristic NOE contacts (Figure 5) and chemical shift changes (Figure 4) suggest that the two transcription activation subdomains of VP16 adopt an  $\alpha$ -helical conformation around the 429–450 and 465–488 regions upon interaction with PC4 and presumably also TFIIB (as indicated by chemical shift changes).

The most pronounced chemical shift changes and the largest decrease in peak intensities upon interaction with PC4 and TFIIB are observed within both VP16 activation subdomains that have previously been reported to be essential for transcription (26, 28, 29). Cress and Triezenberg (28) observed that transcription was only impaired when multiple patches of negative charged residues in VP16ad/n were mutated, suggesting that the overall acidity of the protein is important for its activity. Our docking models explain this observation, since multiple exchangeable contacts are observed between negatively charged VP16 residues and positively charged residues from the target proteins. One specific acidic residue in the VP16ad/c subdomain (E476) significantly contributes to transcriptional activation (29). Mutation of this acidic residue (E474K,E476K mutant, Figure 3B) had the most pronounced effect on the interaction between PC4 and VP16, confirming the importance of this glutamate. The docking results show that this residue often makes a hydrogen bond to R85, which was shown to be critically important for interaction (Jonker et al, manuscript in preparation). The large number of charged residues increases the rate of interaction between activator and target through long-range electrostatic forces. This is in agreement with the observed difference in PC4 binding affinity for the D443K,D445K mutant in comparison with the D443A,D445A mutant (Figure 3B). The docking results show that D443 and D445 mostly make hydrogen bonds to K100' and K77/K79 of PC4, respectively, residues that are important for the interaction (Jonker et al, manuscript in preparation). It is suggested that initial binding occurs by electrostatic interactions, resulting in an unstable complex,

whereas it slowly converts into a more stable and defined complex by specific contacts between the TAD and its target (63). In this respect, specific hydrophobic residues may be important. By NMR, we show that hydrophobic residues, shown to be critical for transcription (L439, F442, L444, F475, F473 and F479 (26, 29)), are in the center of the induced  $\alpha$ -helix. Peak broadening was more pronounced for the area where these residues reside than for the surrounding regions, suggesting close contacts with PC4. The docking results clearly indicate that side-chains of these residues make the most important hydrophobic interactions with PC4. The large  $^1\text{H}\beta$  resonance perturbation of F479 and decrease in binding affinity for F479P point mutation confirm the importance of this residue for interaction. However, we observed that the interaction between PC4 and VP16 is only marginally decreased by the mutants F442P and L444A,L447A, or within the other activation subdomain by the mutant L483P, which is most probably due to the presence of two independent interaction domains, and a relatively large helical interaction surface. Furthermore, destroying part of the helix could be compensated by the presence of other interacting residues within the mutated domain. Indeed, binding of PC4 to VP16 was diminished by deletion of the VP16ad/c subdomain (Figure 3A, ref 20), while only if also F442 within the other subdomain was mutated to proline was a complete loss of interaction observed (20).

**Binding of VP16ad to the General Cofactor PC4.** We propose a model, based on two independent docking approaches using NMR chemical shift perturbations, for the binding of  $\alpha$ -helical VP16ad 465–490 and 430–450 regions to the PC4ctd dimer. The models show binding of the negatively charged VP16  $\alpha$ -helix to the positively charged  $\beta$ -channel regions of PC4 (Figure 6B), which is in agreement with mutational analysis of specific VP16 residues (Figure 3B) and PC4 residues and observed salt concentration dependence of the interaction (Jonker et al, manuscript in preparation). The 474–484 and 444–448 regions, which are mostly affected by binding (Figure 2), are particularly well enclosed and make many electrostatic and some hydrophobic contacts to residues in the  $\beta$ -channel of PC4ctd. Interestingly, the docking results indicate that many contacts can be replaced by adjacent VP16 residues; consequently, complete loss of binding is not observed by mutation of a few polar or hydrophobic residues. Both VP16ad subregions expose a strong negatively charged binding site that allows multiple contact possibilities, which provides an explanation for the cooperativity in interactions and transactivation. The buried surface area for the VP16 activation subdomains ( $1920 \pm 140 \text{ \AA}^2$  for VP16ad/c and  $1410 \pm 140 \text{ \AA}^2$  for VP16ad/n) are comparable with the average protein–protein interaction ( $1600 \pm 400 \text{ \AA}^2$ ) (64). For similar interactions of induced  $\alpha$ -helix formation by activator–target complexes, smaller buried interaction surfaces were found for CREB-p300 ( $\sim 1200 \text{ \AA}^2$ ) (57) and p53-MDM2 ( $\sim 1500 \text{ \AA}^2$ ) (65), while the HIF1  $\alpha$ -p300 complex buries a much larger area ( $\sim 3400 \text{ \AA}^2$ ) (60). The two symmetrical  $\beta$ -channel regions in the PC4ctd dimer may both embrace one VP16 molecule. Analysis of binding data and NMR relaxation data (data not shown) suggest a complex between two PC4 dimers and one or two VP16 molecules. This indicates that the second VP16ad  $\alpha$ -helical region either folds back and contacts the  $\beta$ -channel on the other side of the same dimer or interacts

with a  $\beta$ -channel of another PC4 dimer. At present, we cannot discriminate between these possibilities.

**Binding of VP16ad to the General Transcription Factor TFIIB.** TFIIB is one of the essential factors in RNA polymerase II transcription that enters the PIC after formation of the TBP–DNA complex. Biochemical analysis and NMR have shown before that the amino-terminal zinc binding domain of TFIIB (TFIIBn) and VP16ad interact to the same regions in the carboxy-terminal core domain of TFIIB (TFIIBC) (46, 66). Furthermore, the crystal structure of the TFIIBC–TBP–TATA ternary complex (67) and the NMR titrations of TFIIBC with TBP (42) indicate that this interaction region largely overlaps with the TBP–TATA binding site. The opening between the two repeats of TFIIBC in the TBP–TATA bound crystal structure is larger than in the unbound NMR structure. It is believed that VP16 recruits TFIIB to the PIC and exposes the TBP-binding surface by disruption of the intramolecular interactions in TFIIB. We have performed dockings based on NMR chemical shift perturbations in both VP16ad and TFIIBC (46), which indicate a preferential binding of the VP16 465–490 region at the side of the E1 and E2 helices of TFIIB (Figure 6C). VP16 may promote opening of this region to promote the TFIIBC–TBP–TATA complex formation. Furthermore, binding of VP16ad results in shielding of the positively charged groove, replacing it with a new negatively charged surface area, which might also stimulate complex formation with the TBP–TATA complex. The binding site is in agreement with protease footprinting (51) and mutational analysis (52–54). The buried surface area for interaction with this VP16 region ( $1890 \pm 140 \text{ \AA}^2$ ) is comparable with the average protein–protein interaction ( $1600 \pm 400 \text{ \AA}^2$ ) (64). Interestingly, interaction with VP16ad buries a larger surface area than found for the interface between the two structural similar repeats in the solution structure of TFIIBC ( $\sim 1500 \text{ \AA}^2$ ) (46) and for the less compact crystal structure of the TFIIBC–TBP–TATA complex ( $\sim 600 \text{ \AA}^2$ ) (67).

**Biological Implications of the Conformational Changes in the VP16 Activation Domain.** Lack of folded structure has many advantages for the ability of the protein to bind to its targets (68–70). The substantial backbone and side-chain flexibility enables the protein to overcome steric restrictions and to adapt and consequently enhances binding to various targets and larger interaction surfaces. These intrinsically unstructured proteins (IUPs) generally bind with low specificity and low affinity to their targets and involve fast on/off rates. This may also be advantageous after recruitment of a target protein, when an activator has to leave the complex, to allow PIC formation to proceed. Sign-specific chemical shift changes and NOE contacts show that VP16ad folds (at least partially) as an  $\alpha$ -helix when binding to PC4. The low specificity due to the presence of multiple interaction surfaces of the intrinsically unfolded protein combined with the higher binding affinity for the induced  $\alpha$ -helical structure of the activation subdomains results in a protein that combines these properties. On the basis of docking results using NMR chemical shift perturbations, we propose models for the binding of VP16 to TFIIB and PC4. Although for both targets, interaction is observed toward positively charged regions, the distinct VP16ad binding surface is either composed of parallel  $\beta$ -channels (PC4) or a shallow groove between  $\alpha$ -helices (TFIIB), showing the adaptability of

VP16ad. The dockings further show that different VP16 residues are critically involved in contact with either PC4 or TFIIB. In conclusion, both activation subdomains are highly flexible and adopt an  $\alpha$ -helical conformation upon complex formation. The presence of two large interaction surfaces with multiple different contact sites allows cooperative interaction with many different targets and explains the promiscuous properties of the VP16 activation domain.

## ACKNOWLEDGMENT

Thanks to P. N. Palma for providing BiGGER and C. Dominguez and A. M. Bonvin for useful discussions and setting up the HADDOCK dockings. We also thank H. Th. M. Timmers for providing the TFIIB and TBP plasmids and H. van Aken for DNA sequencing.

## REFERENCES

- Struhl, K. (1996) Chromatin structure and RNA polymerase II connection: implications for transcription, *Cell* 84, 179–182.
- Choy, B., and Green, M. R. (1993) Eukaryotic activators function during multiple steps of preinitiation complex assembly, *Nature* 366, 531–536.
- Tjian, R., and Maniatis, T. (1994) Transcriptional activation: a complex puzzle with few easy pieces, *Cell* 77, 5–8.
- Kingston, R. E., Bunker, C. A., and Imbalzano, A. N. (1996) Repression and activation by multiprotein complexes that alter chromatin structure, *Genes Dev.* 10, 905–920.
- Ptashne, M., and Gann, A. (1997) Transcriptional activation by recruitment, *Nature* 386, 569–577.
- Dalrymple, M. A., McGeoch, D. J., Davison, A. J., and Preston, C. M. (1985) DNA sequence of the herpes simplex virus type 1 gene whose product is responsible for transcriptional activation of immediate early promoters, *Nucleic Acids Res.* 13, 7865–7879.
- Cousens, D. J., Greaves, R., Goding, C. R., and O'Hare, P. (1989) The C-terminal 79 amino acids of the herpes simplex virus regulatory protein, Vmw65, efficiently activate transcription in yeast and mammalian cells in chimeric DNA-binding proteins, *EMBO J.* 8, 2337–2342.
- Triebenbarg, S. J., Kingsbury, R. C., and McKnight, S. L. (1988) Functional dissection of VP16, the trans-activator of herpes simplex virus immediate early gene expression, *Genes Dev.* 2, 718–729.
- Hayes, S., and O'Hare, P. (1993) Mapping of a major surface-exposed site in herpes simplex virus protein Vmw65 to a region of direct interaction in a transcription complex assembly, *J. Virol.* 67, 852–862.
- Stringer, K. F., Ingles, C. J., and Greenblatt, J. (1990) Direct and selective binding of an acidic transcriptional activation domain to the TATA-box factor TFIID, *Nature* 345, 783–786.
- Kobayashi, N., Boyer, T. G., and Berk, A. J. (1995) A class of activation domains interacts directly with TFIIA and stimulates TFIIA-TFIID-promoter complex assembly, *Mol. Cell. Biol.* 15, 6465–6473.
- Kobayashi, N., Horn, P. J., Sullivan, S. M., Triebenbarg, S. J., Boyer, T. G., and Berk, A. J. (1998) DA-complex assembly activity required for VP16C transcriptional activation, *Mol. Cell. Biol.* 18, 4023–4031.
- Lin, Y. S., Ha, I., Maldonado, E., Reinberg, D., and Green, M. R. (1991) Binding of general transcription factor TFIIB to an acidic activating region, *Nature* 353, 569–571.
- Zhu, H., Joliot, V., and Prywes, R. (1994) Role of transcription factor TFIIF in serum response factor-activated transcription, *J. Biol. Chem.* 269, 3489–3497.
- Xiao, H., Pearson, A., Coulombe, B., Truant, R., Zhang, S., Regier, J. L., Triebenbarg, S. J., Reinberg, D., Flores, O., Ingles, C. J., et al. (1994) Binding of basal transcription factor TFIH to the acidic activation domains of VP16 and p53, *Mol. Cell. Biol.* 14, 7013–7024.

16. Uesugi, M., Nyanguile, O., Lu, H., Levine, A. J., and Verdine, G. L. (1997) Induced alpha helix in the VP16 activation domain upon binding to a human TAF, *Science* 277, 1310–1313.
17. Goodrich, J. A., Hoey, T., Thut, C. J., Admon, A., and Tjian, R. (1993) Drosophila TAFII40 interacts with both a VP16 activation domain and the basal transcription factor TFIIB, *Cell* 75, 519–530.
18. Klemm, R. D., Goodrich, J. A., Zhou, S., and Tjian, R. (1995) Molecular cloning and expression of the 32-kDa subunit of human TFIID reveals interactions with VP16 and TFIIB that mediate transcriptional activation, *Proc. Natl. Acad. Sci., U.S.A.* 92, 5788–5792.
19. Kretzschmar, M., Kaiser, K., Lottspeich, F., and Meisterernst, M. (1994) A novel mediator of class II gene transcription with homology to viral immediate-early transcriptional regulators, *Cell* 78, 525–534.
20. Ge, H., and Roeder, R. G. (1994) Purification, cloning, and characterization of a human coactivator, PC4, that mediates transcriptional activation of class II genes, *Cell* 78, 513–523.
21. Hardy, S., Brand, M., Mittler, G., Yanagisawa, J., Kato, S., Meisterernst, M., and Tora, L. (2002) TATA-binding protein-free TAF-containing complex (TFTC) and p300 are both required for efficient transcriptional activation, *J. Biol. Chem.* 277, 32875–32882.
22. Ikeda, K., Stuehler, T., and Meisterernst, M. (2002) The H1 and H2 regions of the activation domain of herpes simplex virion protein 16 stimulate transcription through distinct molecular mechanisms, *Genes Cells* 7, 49–58.
23. Kraus, W. L., Manning, E. T., and Kadonaga, J. T. (1999) Biochemical analysis of distinct activation functions in p300 that enhance transcription initiation with chromatin templates, *Mol. Cell. Biol.* 19, 8123–8135.
24. Kundu, T. K., Palhan, V. B., Wang, Z., An, W., Cole, P. A., and Roeder, R. G. (2000) Activator-dependent transcription from chromatin in vitro involving targeted histone acetylation by p300, *Mol. Cell.* 6, 551–561.
25. Seipel, K., Georgiev, O., and Schaffner, W. (1992) Different activation domains stimulate transcription from remote ('enhancer') and proximal ('promoter') positions, *EMBO J.* 11, 4961–4968.
26. Regier, J. L., Shen, F., and Triezenberg, S. J. (1993) Pattern of aromatic and hydrophobic amino acids critical for one of two subdomains of the VP16 transcriptional activator, *Proc. Natl. Acad. Sci., U.S.A.* 90, 883–887.
27. Walker, S., Greaves, R., and O'Hare, P. (1993) Transcriptional activation by the acidic domain of Vmw65 requires the integrity of the domain and involves additional determinants distinct from those necessary for TFIIB binding, *Mol. Cell. Biol.* 13, 5233–5244.
28. Cress, W. D., and Triezenberg, S. J. (1991) Critical structural elements of the VP16 transcriptional activation domain, *Science* 251, 87–90.
29. Sullivan, S. M., Horn, P. J., Olson, V. A., Koop, A. H., Niu, W., Ebright, R. H., and Triezenberg, S. J. (1998) Mutational analysis of a transcriptional activation region of the VP16 protein of herpes simplex virus, *Nucleic Acids Res.* 26, 4487–4496.
30. Triezenberg, S. J. (1995) Structure and function of transcriptional activation domains, *Curr. Opin. Genet. Dev.* 5, 190–196.
31. Wright, P. E., and Dyson, H. J. (1999) Intrinsically unstructured proteins: re-assessing the protein structure–function paradigm, *J. Mol. Biol.* 293, 321–331.
32. O'Hare, P., and Williams, G. (1992) Structural studies of the acidic transactivation domain of the Vmw65 protein of herpes simplex virus using 1H NMR, *Biochemistry* 31, 4150–4156.
33. Grossmann, J. G., Sharff, A. J., O'Hare, P., and Luisi, B. (2001) Molecular shapes of transcription factors TFIIB and VP16 in solution: implications for recognition, *Biochemistry* 40, 6267–6274.
34. Werten, S., Langen, F. W., van Schaik, R., Timmers, H. Th. M., Meisterernst, M., and van der Vliet, P. C. (1998) High-affinity DNA binding by the C-terminal domain of the transcriptional coactivator PC4 requires simultaneous interaction with two opposing unpaired strands and results in helix destabilization, *J. Mol. Biol.* 276, 367–377.
35. Werten, S., Wechselberger, R., Boelens, R., van der Vliet, P. C., and Kaptein, R. (1999) Identification of the single-stranded DNA binding surface of the transcriptional coactivator PC4 by NMR, *J. Biol. Chem.* 274, 3693–3699.
36. Folkers, G. E., van Buuren, B. N. M., and Kaptein, R. (2004) Expression screening, protein purification and NMR analysis of human protein domains for structural genomics, *J. Struct. Funct. Genomics* 5, 119–131.
37. Cavanagh, J., Fairbrother, W. J., Palmer III, A. G., and Skelton, N. J. (1996) *Protein NMR Spectroscopy*, Academic Press, San Diego, CA.
38. Delaglio, F., Grzesiek, S., Vuister, G. W., Zhu, G., Pfeifer, J., and Bax, A. (1995) NMRPipe: a multidimensional spectral processing system based on UNIX pipes, *J. Biomol. NMR* 6, 277–293.
39. Morelli, X. J., Palma, P. N., Guerlesquin, F., and Rigby, A. C. (2001) A novel approach for assessing macromolecular complexes combining soft-docking calculations with NMR data, *Protein Sci.* 10, 2131–2137.
40. Palma, P. N., Krippahl, L., Wampler, J. E., and Moura, J. J. (2000) BiGGER: a new (soft) docking algorithm for predicting protein interactions, *Proteins* 39, 372–384.
41. Brandsen, J., Werten, S., van der Vliet, P. C., Meisterernst, M., Kroon, J., and Gros, P. (1997) C-terminal domain of transcription cofactor PC4 reveals dimeric ssDNA binding site, *Nat. Struct. Biol.* 4, 900–903.
42. Bagby, S., Kim, S., Maldonado, E., Tong, K. I., Reinberg, D., and Ikura, M. (1995) Solution structure of the C-terminal core domain of human TFIIB: similarity to cyclin A and interaction with TATA-binding protein, *Cell* 82, 857–867.
43. Guex, N., and Peitsch, M. C. (1997) SWISS-MODEL and the Swiss-PdbViewer: an environment for comparative protein modeling, *Electrophoresis* 18, 2714–2723.
44. van Gunsteren, W. F., Billeter, S. R., Eising, A. A., Hünenberger, P. H., Krüger, P., Mark, A. E., Scott, W. R. P., and Tironi, I. G. (1996) Biomolecular simulation: The GROMOS96 manual and user guide, Vdf Hochschulverlag, Zürich, Switzerland.
45. Dominguez, C., Boelens, R., and Bonvin, A. M. (2003) HADDOCK: a protein–protein docking approach based on biochemical or biophysical information, *J. Am. Chem. Soc.* 125, 1731–1737.
46. Hayashi, F., Ishima, R., Liu, D., Tong, K. I., Kim, S., Reinberg, D., Bagby, S., and Ikura, M. (1998) Human general transcription factor TFIIB: conformational variability and interaction with VP16 activation domain, *Biochemistry* 37, 7941–7951.
47. Koradi, R., Billeter, M., and Wuthrich, K. (1996) MOLMOL: a program for display and analysis of macromolecular structures, *J. Mol. Graph.* 14, 51–55, 29–32.
48. Wang, Y., and Jardetzky, O. (2002) Probability-based protein secondary structure identification using combined NMR chemical-shift data, *Protein Sci.* 11, 852–861.
49. Wishart, D. S., and Sykes, B. D. (1994) The <sup>13</sup>C chemical-shift index: a simple method for the identification of protein secondary structure using <sup>13</sup>C chemical-shift data, *J. Biomol. NMR* 4, 171–180.
50. Cornilescu, G., Delaglio, F., and Bax, A. (1999) Protein backbone angle restraints from searching a database for chemical shift and sequence homology, *J. Biomol. NMR* 13, 289–302.
51. Hori, R., Pyo, S., and Carey, M. (1995) Protease footprinting reveals a surface on transcription factor TFIIB that serves as an interface for activators and coactivators, *Proc. Natl. Acad. Sci., U.S.A.* 92, 6047–6051.
52. Roberts, S. G., Ha, I., Maldonado, E., Reinberg, D., and Green, M. R. (1993) Interaction between an acidic activator and transcription factor TFIIB is required for transcriptional activation, *Nature* 363, 741–744.
53. Gupta, R., Emili, A., Pan, G., Xiao, H., Shales, M., Greenblatt, J., and Ingles, C. J. (1996) Characterization of the interaction between the acidic activation domain of VP16 and the RNA polymerase II initiation factor TFIIB, *Nucleic Acids Res.* 24, 2324–2330.
54. Chou, S., and Struhl, K. (1997) Transcriptional activation by TFIIB mutants that are severely impaired in interaction with promoter DNA and acidic activation domains, *Mol. Cell. Biol.* 17, 6794–6802.
55. Shen, F., Triezenberg, S. J., Hensley, P., Porter, D., and Knutson, J. R. (1996) Transcriptional activation domain of the herpesvirus protein VP16 becomes conformationally constrained upon interaction with basal transcription factors, *J. Biol. Chem.* 271, 4827–4837.
56. Sadowski, I., Ma, J., Triezenberg, S., and Ptashne, M. (1988) GAL4-VP16 is an unusually potent transcriptional activator, *Nature* 335, 563–564.

57. Radhakrishnan, I., Perez-Alvarado, G. C., Parker, D., Dyson, H. J., Montminy, M. R., and Wright, P. E. (1997) Solution structure of the KIX domain of CBP bound to the transactivation domain of CREB: a model for activator: coactivator interactions, *Cell* 91, 741–752.
58. Lee, H., Mok, K. H., Muhandiram, R., Park, K. H., Suk, J. E., Kim, D. H., Chang, J., Sung, Y. C., Choi, K. Y., and Han, K. H. (2000) Local structural elements in the mostly unstructured transcriptional activation domain of human p53, *J. Biol. Chem.* 275, 29426–29432.
59. Zor, T., Mayr, B. M., Dyson, H. J., Montminy, M. R., and Wright, P. E. (2002) Roles of phosphorylation and helix propensity in the binding of the KIX domain of CREB-binding protein by constitutive (c-Myb) and inducible (CREB) activators, *J. Biol. Chem.* 277, 42241–42248.
60. Freedman, S. J., Sun, Z. Y., Poy, F., Kung, A. L., Livingston, D. M., Wagner, G., and Eck, M. J. (2002) Structural basis for recruitment of CBP/p300 by hypoxia-inducible factor-1 alpha, *Proc. Natl. Acad. Sci., U.S.A.* 99, 5367–5372.
61. Dames, S. A., Martinez-Yamout, M., De Guzman, R. N., Dyson, H. J., and Wright, P. E. (2002) Structural basis for Hif-1 alpha /CBP recognition in the cellular hypoxic response, *Proc. Natl. Acad. Sci., U.S.A.* 99, 5271–5276.
62. Uesugi, M., and Verdine, G. L. (1999) The alpha-helical FXX-PhiPhi motif in p53: TAF interaction and discrimination by MDM2, *Proc. Natl. Acad. Sci., U.S.A.* 96, 14801–14806.
63. Hermann, S., Berndt, K. D., and Wright, A. P. (2001) How transcriptional activators bind target proteins, *J. Biol. Chem.* 276, 40127–40132.
64. Lo Conte, L., Chothia, C., and Janin, J. (1999) The atomic structure of protein–protein recognition sites, *J. Mol. Biol.* 285, 2177–2198.
65. Kussie, P. H., Gorina, S., Marechal, V., Elenbaas, B., Moreau, J., Levine, A. J., and Pavletich, N. P. (1996) Structure of the MDM2 oncoprotein bound to the p53 tumor suppressor transactivation domain, *Science* 274, 948–953.
66. Roberts, S. G., and Green, M. R. (1994) Activator-induced conformational change in general transcription factor TFIIB, *Nature* 371, 717–720.
67. Nikolov, D. B., Chen, H., Halay, E. D., Usheva, A. A., Hisatake, K., Lee, D. K., Roeder, R. G., and Burley, S. K. (1995) Crystal structure of a TFIIB-TBP-TATA-element ternary complex, *Nature* 377, 119–128.
68. Dunker, A. K., Lawson, J. D., Brown, C. J., Williams, R. M., Romero, P., Oh, J. S., Oldfield, C. J., Campen, A. M., Ratliff, C. M., Hipps, K. W., Ausio, J., Nissen, M. S., Reeves, R., Kang, C., Kissinger, C. R., Bailey, R. W., Griswold, M. D., Chiu, W., Garner, E. C., and Obradovic, Z. (2001) Intrinsically disordered protein, *J. Mol. Graph. Model.* 19, 26–59.
69. Dunker, A. K., Brown, C. J., Lawson, J. D., Iakoucheva, L. M., and Obradovic, Z. (2002) Intrinsic disorder and protein function, *Biochemistry* 41, 6573–6582.
70. Tompa, P. (2002) Intrinsically unstructured proteins, *Trends Biochem. Sci.* 27, 527–533.
71. Vis, H., Boelens, R., Mariani, M., Stroop, R., Vorgias, C. E., Wilson, K. S., and Kaptein, R. (1994) <sup>1</sup>H, <sup>13</sup>C, and <sup>15</sup>N resonance assignments and secondary structure analysis of the HU protein from *Bacillus stearothermophilus* using two- and three-dimensional double- and triple-resonance heteronuclear magnetic resonance spectroscopy, *Biochemistry* 33, 14858–14870.

BI0482912